Optimizing the Potential of BR Slag in Blended Cement

Michiel Giels[1], Tobias Hertel[2], Marcus Sommerfeld[3], Christian Dertmann[4], Bernd Friedrich[5] and Yiannis Pontikes[6]
1. PhD student
2. Postdoctoral researcher
3. Project manager
4. PhD student
5. Professor of IME Process Metallurgy and Metal Recycling
6. Professor of Sustainable Resources for Engineered Materials (SREMat)
KU Leuven 1,2,6, Department of Metallurgy and Materials Engineering, Leuven, Belgium.
RWTH 3,4,5, IME Process Metallurgy and Metal Recycling, Aachen, Germany
Corresponding author: michiel.giels@kuleuven.be

Abstract

Bauxite residue (BR) has in principle a great potential to be used in the construction industry considering its large availability. However, BR originating from the Bayer process lacks reactivity, i.e., hydraulic/pozzolanic activity in alkaline conditions, which is required in cementitious applications. Therefore, BR is commonly heat treated through either calcination (<1000 °C), (partial) vitrification (1100 - 1300 °C) or smelting combined with iron extraction (1500 - 1700 °C) to form crystalline or amorphous phases that are soluble at neutral or high pH. Smelting of BR is of much interest as it offers the advantage of combining both metal recovery and valorization of the slag as supplementary cementitious material. However, it has been shown that the purity of the metal and the price of the slag is crucial for the financial feasibility of the process. In this work, the potential of the slag for its use in blended cement was investigated and compared to blast furnace slag (BFS), which is considered a high value supplementary cementitious material. A mix of BR (>80 wt.%), SiO_2, CaO and C was treated in an electric-arc furnace (EAF) at 1550 – 1600 °C to form slag (EAFS) and pig iron. The reactivity of the EAFS was found to be significantly higher than BFS in a simulated cementitious environment. Optimization of the mix design showed that a similar 7 and 28 d strength to 100 % Portland cement (PC) could be obtained using only 55 wt.% PC, 30 wt.% EAF slag and 15 wt.% limestone. The latter shows that EAFS has large potential as supplementary cementitious material and should be considered for further investigation.

Keywords: Bauxite residue, Slag, Glass, Reactivity, Blended cement.

1. Introduction

Supplementary cementitious materials (SCMs) are crucial to reduce the amount of Portland cement (PC) for economic and environmental reasons. These materials are blended with PC and are classified as either pozzolanic (react with $Ca(OH)_2$ and water) or latent hydraulic (reacting with water) for the formation of cementitious hydrates and have the benefit of increasing the late age strength development, durability and reduction in thermal cracking [1]. Blast furnace slag (BFS), fly ashes and limestone are the SCMs that are already widely used [2]. However, due to the climate transition, processes for the production of BFS and fly ash will change and reduce significantly its availability [3]. Surprisingly, this is in contrast with the enormous pressure to decarbonize the cement industry, which actually requires a larger amount of SCMs [3–5]. Bauxite residue (BR) could play a vital role as SCM due to it large locally available volumes. However, currently BR originating from the Bayer process is only used as Fe and Al source in the production of PC (< 5 wt.%) and is not considered as SCM [6]. Major reasons are the alkaline nature, being

classified as (hazardous) waste, small particle size, and from a technical point of view its low reactivity (hydraulic/pozzolanic activity), e.g., in a cementitious environment [7].

Bayer already mentioned in his original process patent the potential for iron recovery from bauxite residue [8]. Extraction of iron would require a carbothermic reduction for the production of pig iron (1500 – 1700 °C) or a low temperature reduction for the formation of magnetite through alkali roasting [9] or H_2 reduction [10], which can be later converted to pig iron. It has been shown that direct carbothermic reduction of BR with an electric arc furnace (EAF) is feasible at lab [11] and pilot scale [12]. Because an EAF requires a large amount of energy, the valorization of the extracted slag is crucial to make the process profitable [12]. However, the slag was mainly investigated for Al, Ti or rare earth recovery [11,13,14] and as the slag can be granulated, resulting in an fully amorphous material, it is actually of much interest as cement replacement in concrete and mortars. If a precursor with similar reactivity to BFS could be obtained, the potential is enormous as BFS is considered a high value SCM nowadays with similar price as PC with demand expected to increase in the near future.

This work investigated the treatment of BR in an EAF, with the focus of optimizing the reactivity of the slag phase. The optimal mix of fluxes, reported in Giels et al. [15] for vitrification of BR, was used as it has been shown to result in a reactive amorphous phase. Only partial reduction of Fe was targeted as Fe^{2+} has a positive effect on the depolymerization degree of the glass [16,17], which can increase the reactivity as SCM. This way of thinking deviates from traditional concepts by minimizing the addition of Ca or Mg through substitution with Fe. This can decrease the CO_2 footprint of the process considerably as Ca and Mg are commonly added as carbonates. The reactivity of the EAF slag (EAFS) was afterwards evaluated using the rapid, relevant and reliable (R^3) reactivity test method, which allows to measure the reaction degree of materials in a simulated cementitious environment. Using the data of the R^3 test, the mix design of a blended cement was optimized with respect to compressive and flexural strength. Finally, the reactivity of the EAF slag was compared to BFS and its potential discussed.

2. Methodology

2.1 Characterization and Processing

BR slurry originating from the Tulcea plant was filtrated and the solid BR was dried at 300 °C for 24 h and milled below 500 µm using a rotary disk mill. After drying, the LOI was measured through thermogravimetric analysis (TGA) using a TA SDT Q600 up to 1000 °C with a heating rate of 10°C/min under nitrogen atmosphere. The chemical analysis of the residues was performed using a Bruker S8 Tiger Wavelength Dispersive X-ray fluorescence spectrometer (WDXRF) following a lithium borate and lithium bromide fusion with 10 wt.% BR sample at 1050 °C to form fusion beads.

BR was mixed with CaO and SiO_2 in the weight ratio BR:CaO:SiO_2:C as 100:10:10:3.6 g. The amount of CaO and SiO_2 was based on the work of Giels et al. [15]. Carbon was fluxed under the stoichiometric ratio to keep as much as Fe^{2+} in the slag. Smelting was conducted in a refractory lined 100 kVA DC EAF, within a graphite crucible (Figure 1A). Experiments were triplicated and the material was heated till 1550-1600 °C and the melt was held for 31, 20 and 11 min, respectively. Afterwards, the slag was poured in water as shown in Figure 1B and was dried at 105 ± 5 °C for 24 h. Remaining metallic iron was removed through dry magnetic separation using a Nd magnet. Metallic iron at the bottom of the crucible was solidified in the crucible.

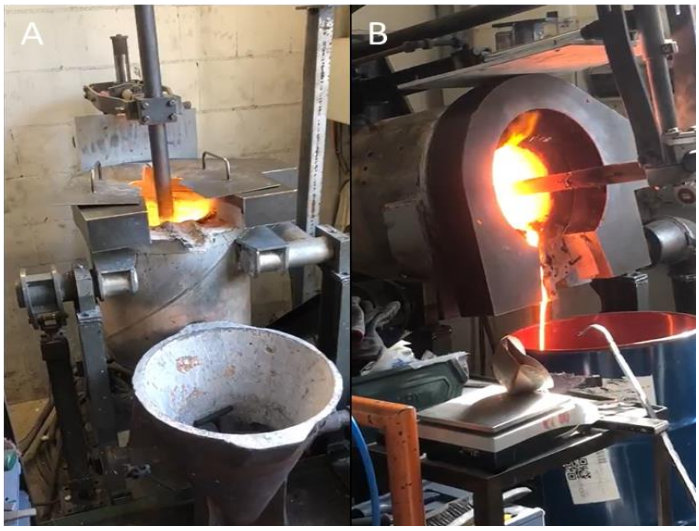

Figure 1A. Smelting of the BR mix with the EAF and Figure 1B. Quenching of the slag in water.

2.2 Characterization

The metal was after cooling, cut, ground and polished. The chemistry was determined through wavelength dispersive X-ray fluorescence (WDXRF) (AXIOS^{mAX}). Carbon and sulfur were measured using a combustion method and coupled infrared measurement cells using drilling chips of the metal (ELTRA CS 2000). EAFS was dried at 105 °C, and homogenized and milled in an attritor ball mill 1S to a specific surface area of 4400 ± 200 cm²/g, measured according to EN 196-6. The mineralogy was characterized through X-ray diffraction (XRD) using a Cu source with Kα radiation of 30 kV and 10 mA in the range of 5-70° 2 theta, with a step size of 0.02° and time step of 1 s.

2.3 Reactivity Test

Milled EAFS and a commercially available BFS from ECOCEM with a Blaine of 4320 ± 200 cm²/g were subjected to the R³ calorimeter reactivity test method, according to [19–21]. This test method simulates the reaction of an SCM in a simulated cement environment. The heat release is in this test closely related to compressive strength and can be used as a reliable indicator for the performance in a blended cement system. Details of this procedure can be found in [19–21]. Hydration of the R^3 pastes was stopped through a solvent exchange and analysed using XRD, TGA and differential TGA (DTG). TGA allowed to calculate the bound water content (25 - 350°C) and amount of portlandite consumed $Ca(OH)_2$ of the pastes samples.

2.4 Mortar Production

Mortars containing PC (CEM I 52.5 R), EAFS, limestone and gypsum were produced and cured according to EN 196-1 [22]. The flow of all mortars was measured through the flow table test according to EN 1015-3. The compressive and flexural strength of the mortar blocks was tested after 2, 7 and 28 d curing, using an Instron 5985 testing machine with a load rate of 2 and 0.5 mm/min, respectively.

3. Results and Discussion

3.1 Characterization of Slag and Metal

The chemistry of the dried BR is shown below in Table 1.. The BR was rich in Fe_2O_3 and Al_2O_3, which is on average close to the reported chemistries for BR originating from the Bayer process [23].

Table 1. Chemistry of the lithium borate beads measured through WDXRF using matrix matched standards. LOI measured through TGA (1000 °C).

	Fe_2O_3	**Al_2O_3**	**SiO_2**	**CaO**	**TiO_2**	**Na_2O**	**Other**	**LOI**
	[wt.%]	[wt.%]	[wt.%]	[wt.%]	[wt.%]	[wt.%]	[wt.%]	[wt.%]
BR	46.0 ± 0.2	22.3 ± 0.3	14.0 ± 0.1	5.0 ± 0.0	3.6 ± 0.0	8.8 ± 0.0	0.2 ± 0.0	11.7

The mix of BR with CaO, SiO_2 and C fluxes was heated till 1550-1600 °C in the EAF. Thermodynamic calculations using FactSage™ [24] showed that theoretically only 5 wt.% of metal would form during processing. However, during the experiment 25 wt.% of metal was precipitated. This is attributed to the interaction of the melt with the graphite crucible and electrode. The slag on top of the liquid metal was cooled in water and the metal at the bottom was slowly solidified in the crucible after the experiment. The chemistry of the metal phase can be found in Table 2 and indicates that the precipitated metal is pig iron. Table 3 shows the chemistry of the EAFS including other materials used in this work such as the BFS reference and PC (CEM I 52.5R). The EAFS is characterized by a depleted Fe content (10.9 wt.%), due to the precipitation of pig iron. Due to the extraction of the iron, all the other elements present in the BR are enriched in the slag.

Table 2. Chemistry of the metal phase measured through WDXRF.

	Fe	**P**	**Cr**	**Cu**	**Ni**	**Al**	**C**	**S**
	[wt.%]	[wt.%]	[wt.%]	[wt.%]	[wt.%]	[wt.%]	[wt.%]	[wt.%]
Metal	95.06	0.14	0.07	0.03	0.03	0.02	4.47 ± 0.1	0.13 ± 0

The chemistry of the produced EAFS and a commercial BFS, used as reference in this work, is shown in Table 2. The FeO content in the EAFS was quite low with respect to the original BR as Fe was extracted as pig iron. The EAFS has a significantly larger Al_2O_3, Na_2O and FeO content, but lower CaO and SiO_2 content compared to BFS. The chemistry of the EAFS can be considered as quite unique, but would be not considered as an interesting SCM according to the relevant norms such as EN 197-1 due to the low amount of CaO, MgO and SiO_2 (<67 wt.%), and low ratio of CaO/SiO_2 (<1). The XRD of the EAFS and BFS can be found Figure 2 and show the full amorphous nature of both materials.

Table 3. Chemistry of BFS and EAFS.

	EAFS	BFS
	[wt.%]	[wt.%]
FeO	10.9	0.5
CaO	21.9	44.8
Al_2O_3	25.3	11.2
SiO_2	24.3	33.0
TiO_2	3.7	0.7
MgO	0.2	6.8
Na_2O	12.7	0.3
Others	1.0	2.7

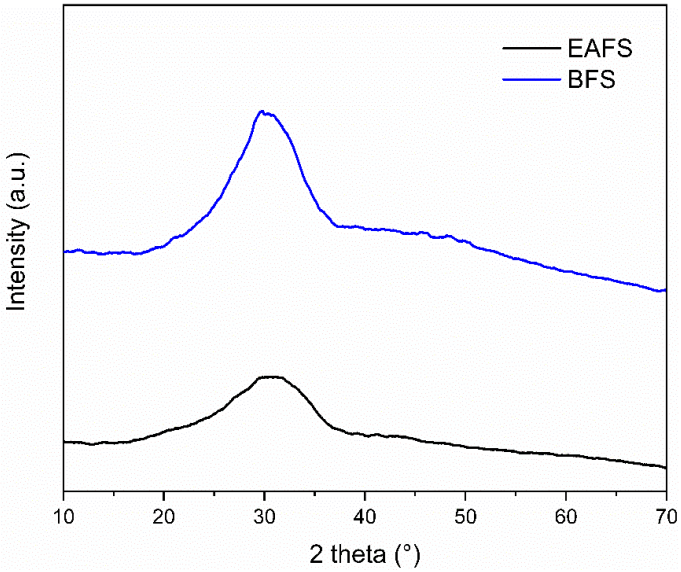

Figure 2. XRD of EAFS and BFS.

3.2 Reactivity Test

Figure 3 shows the heat release in the R^3 test of the EAFS and BFS. EAFS shows a faster heat release and significant higher overall heat with respect to BFS. Figure 4 shows the DTG and XRD of the EAFS R^3 paste after 7 days. In DTG, a first hump at 130 °C could be assigned to the AFm phases, which was identified in XRD as monosulfate (Ms), carbonated hemi- (Hc) and monocarboaluminate (Mc) [25,26]. Further a hump at 250 °C to 350 °C in DTG, could be linked to Mc and silicious hydrogarnet (Hdg) in XRD [25,27]. The background in the DTG most likely also indicates the presence of a hydrate gel such as C-(A)-(F)-S-H [25].

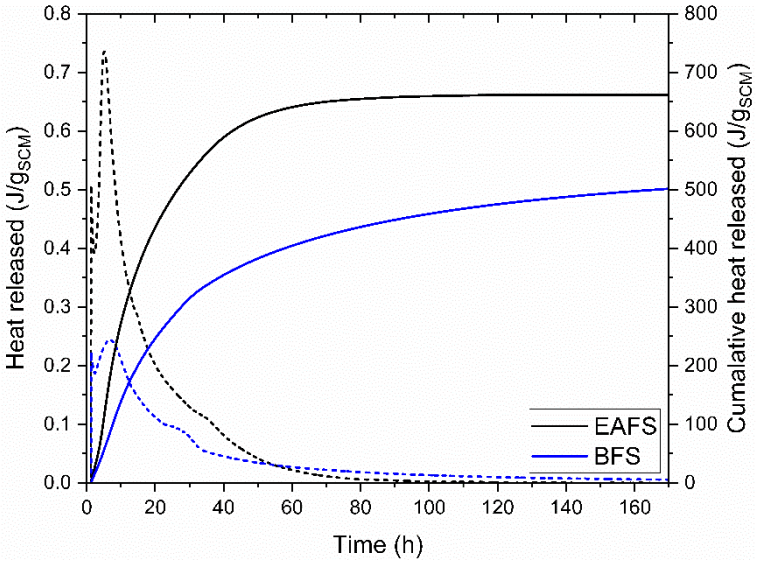

Figure 3. Heat released of EAFS and BFS in the R3 test.

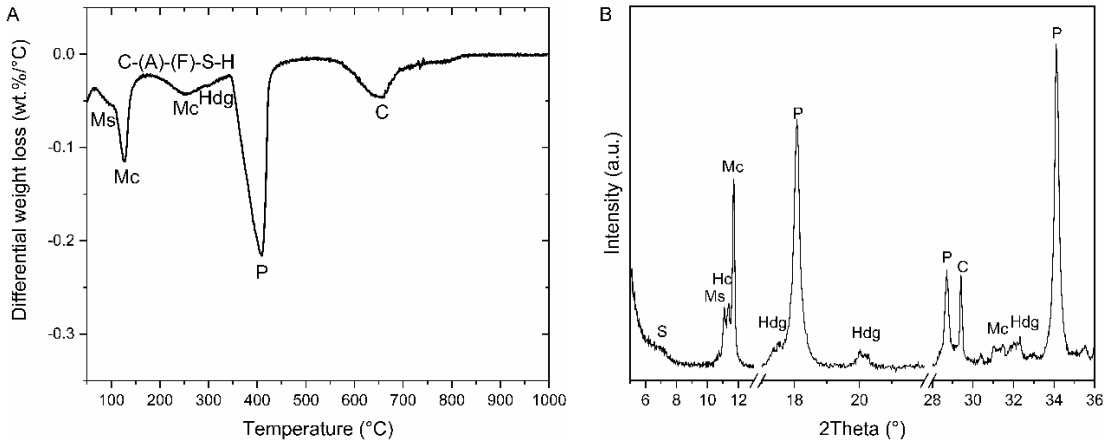

Figure 4. A) DTG and B) XRD of solvent exchanged R3 pastes with Ms: Monosulfate, Hc: Carbonated Hemicarboaluminate, Mc: Monocarboaluminate, P: Portlandite, C: Calcite, C-S-H: Calcium silicate hydrate gel and Hdg: Silicious hydrogarnet.

Table 4shows that significant amount of water is bound and Ca $(OH)_2$ is consumed in the R^3 test. This is important as the phases formed can minimize porosity by the bounding of water and therefore increase the strength in a blended cement. The increase in bound water and heat can be attributed to the formation of Mc (1), Hc (2), Ms (3) and C-(A)-(F)-S-H. EAFS is therefore mainly contributing to the formation of voluminous phases by providing Al, Ca, Fe and Si. The R^3 data indicates that the addition of calcite is key as Hc and Mc are highly desirable phases in cementitious binders as they not only contribute to strength, but also stabilize the AFt phase [27].

$$4Ca^{2+} + 2Al(OH)_4^- + CO_3^{2-} + 4OH^- + 5H_2O = 3CaO \cdot Al_2O_3 \cdot (CaCO_3) \cdot 11H_2O(s) \quad (1)$$

$$4Ca^{2+} + 2Al(OH_4^- + 0.5CO_3^{2-} + 5OH^- + 5.5H_2O = 3CaO \cdot Al_2O_3(Ca(OH)_2)_{0.5} \cdot (CaCO_3)_{0.5}11.5H_2O(s) \quad (2)$$

$$4Ca^{2+} + 2Al(OH)_4^- + SO_4^{2-} + 4OH^- + 4.5H_2O = 3CaO \cdot Al_2O_3 \cdot (CaSO_4) \cdot 10.5H_2O(s) \quad (3)$$

The phases formed and high heat recorded in the R^3 test indicate that a blended cement with EAFS could contribute significantly to strength. According to the correlations of R^3 and strength of

mortars [20], a 30 wt.% replacement would result in higher 7 and 28 day strength than the reference cement as shown in Table 4. This would mean that EAFS would have a larger potential than BFS to contribute to strength.

Table 4. Calculated bound water and consumed $Ca(OH)_2$ using TGA data and predicted strength (if 30 wt.% of PC is replaced) using the cumulative heat of the R3 test [20].

	Bound water (<350 °C)	$Ca(OH)_2$ consumed	Rel. 28 d Strength (72h)	Rel. 28 d Strength (168h)
	[g/100 g dry paste]	[g/100 g SCM]	[%]	[%]
EAFS	13.5	87.9	9	7

3.3 Mortar Production

The mix design and mortar flow of the cement mortars is shown in Table 5. A partial replacement of cement with limestone was considered as improved properties were reported for Al rich SCMs such as metakaolin [27,28]. Various amounts of gypsum were added to see if a beneficial effect could be observed on the properties. It can be observed that the addition of EAFS slightly improved the mortar flow, although its density (2.8 g/cm³) is much lower than PC (3.15 g/cm³).

Table 6: Mix design blended cement mortars according to EN 196 -1 with weights normalized to 100 g and its respective flow.

	PC	**EAFS**	**Limestone**	**Gypsum**	**Water**	**Sand**	**Mortar flow**
	[g]	[g]	[g]	[g]	[g]	[g]	[mm]
100 PC	100	-	-	-	50	300	191
70PC 30EAFS 1G	69	30	-	1	50	300	195
70PC 30EAFS 3G	68	29	-	3	50	300	194
55PC 30EAFS 15Cc 0G	55	30	15	0	50	300	198
55PC 30EAFS 15Cc 1G	54	30	15	1	50	300	197
55PC 30EAFS 15Cc 5G	53	29	15	3	50	300	196

Figure 5A and B show the compressive and flexural strength of the blended cement mortars. The replacement of 30 wt.% PC by EAFS resulted in a similar 7 and 28 d compressive strength to 100 wt.% PC. This was also observed in the work of [14], which used the EAFS produced in this work. The replacement of additional PC (45 wt.%) by limestone, resulted in a similar strength and indicates the important synergy between limestone and EAFS. The high strength can be linked to the formation of HC, Mc and C-(A)-(S)-H by the pozzolanic reaction of EAFS as observed by the R^3 test and stabilization of ettringite by Hc and Mc [27,28]. This makes it quite similar to LC^3 cement, although no superplasticizer was required. The addition of gypsum negatively influenced the compressive strength. Figure 8B shows that replacement of PC resulted in higher flexural strength, especially when limestone was included, with respect to the reference PC.

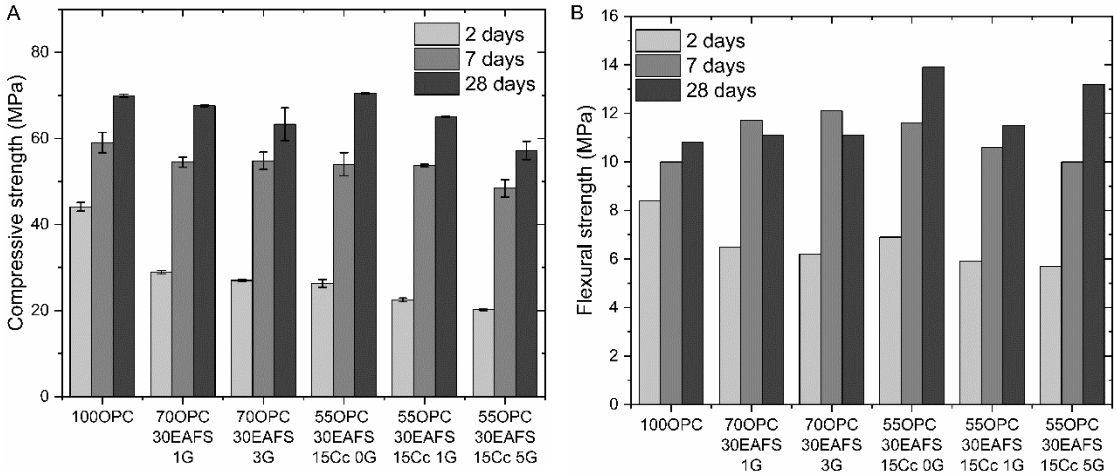

Figure 5. A) Compressive strength of mortars with standard deviation as error bars B) flexural strength of mortars.

3.4 Implications

The results indicate that EAFS is a highly reactive SCM, although the composition is not within the range of traditional SCMs. This shows the limitation of prescriptive based building standards and is another argument for rethinking towards performance-based standards. The observed synergy with limestone is highly desirable as the cement industry is targeting to significantly increase the latter in the blend for the purpose of decarbonizing the industry [4]. According to EN 197-1, the strength of the mortars would be categorized as within the 52.5 N range and could be an alternative to CEM III (PC-BFS) cement. New trials in collaboration with MYTL and RWTH (IME) allowed to produce larger batches, which will be analyzed by research institutes and cement industry for a wide range of properties such as durability.

4. Conclusions

This work explored the potential of BR smelting slag as SCM. A mix of BR (>80 wt.%), CaO and SiO_2 was carbothermic reduced in an EAF at 1550 – 1600 °C. A fully amorphous Fe-rich slag EAFS and pig iron were produced. It was revealed that the finely milled EAFS exhibited a significantly higher reactivity in a simulated cementitious environment (R^3 test) with respect to BFS, a well-established SCM. Optimization of the cement blend revealed an important synergy between limestone and EAFS. An optimum mortar mix consisting of only 55 wt.% PC, 30 wt.% EAFS and 15 wt.% limestone as binder resulted in a similar 7 and 28 d compressive strength as 100 wt.% PC with the benefit of improved workability. The high strength of the mortar could be attributed to the formation of different AFm phases and C-(A)-(F)-S-H gel. These results reveal the large potential of Fe-rich BR smelting slag as high added value SCM. It is therefore of much interest to explore further the potential of the slag in the future.

Acknowledgements

The research leading to these results has been performed within the REMOVAL project and received funding from the European Community's Horizon 2020 Program (H2020/2014-2020) under grant agreement no. 776469.

5. References

1. Ruben Snellings, Gilles Mertens, Jan Elsen, Supplementary cementitious materials, *Rev. Mineral. Geochemistry*. 74 (2012) 211–278. https://doi.org/10.2138/rmg.2012.74.6.
2. K. Scrivener et al., A sustainable future for the european cement and concrete industry, 2019.
3. Maria C.G. Juenger, Ruben Snellings, Susan A. Bernal, Supplementary cementitious materials: New sources, characterization, and performance insights, *Cem. Concr.* Res. 122 (2019) 257–273. https://doi.org/10.1016/j.cemconres.2019.05.008.
4. Ellis Gartner, Hiroshi Hirao, A review of alternative approaches to the reduction of CO2 emissions associated with the manufacture of the binder phase in concrete, *Cem. Concr. Res*. 78 (2015) 126–142. https://doi.org/10.1016/j.cemconres.2015.04.012.
5. Ellis Gartner, Tongbo Sui, Alternative cement clinkers, *Cem. Concr. Res*. 114 (2018) 27–39. https://doi.org/10.1016/j.cemconres.2017.02.002.
6. Y. Pontikes, G.N. Angelopoulos, Bauxite residue in cement and cementitious applications : Current status and a possible way forward, *Resources, Conserv. Recycl*. 73 (2013) 53–63. https://doi.org/10.1016/j.resconrec.2013.01.005.
7. Tobias Hertel, Yiannis Pontikes, Geopolymers, inorganic polymers, alkali-activated materials and hybrid binders from bauxite residue (red mud) – Putting things in perspective, *J. Clean. Prod.* 258 (2020) 120610. https://doi.org/10.1016/j.jclepro.2020.120610.
8. C. Klauber, M. Gräfe, G. Power, Bauxite residue issues: II. options for residue utilization, *Hydrometallurgy.* 108 (2011) 11–32. https://doi.org/10.1016/j.hydromet.2011.02.007.
9. Chenna Rao Borra et al., Comparative Analysis of Processes for Recovery of Rare Earths from Bauxite Residue, *J. Miner. Met. Mater. Soc*. 68 (2016) 2958–2962. https://doi.org/10.1007/s11837-016-2111-y.
10. M. Samouhos et al., Controlled reduction of red mud by H2 followed by magnetic separation, *Miner. Eng.* 105 (2017) 36–43. https://doi.org/10.1016/j.mineng.2017.01.004.
11. Frank Kaußen, Bernd Friedrich, Reductive smelting of red mud for iron recovery, *Chemie-Ingenieur-Technik*. 87 (2015) 1535–1542. https://doi.org/10.1002/cite.201500067.
12. Efthymios Balomenos et al., Mud2Metal: Lessons Learned on the Path for Complete Utilization of Bauxite Residue Through Industrial Symbiosis, *J. Sustain. Metall*. 3 (2016) 551–560. https://doi.org/10.1007/s40831-016-0110-4.
13. Chenna Rao Borra et al., Smelting of bauxite residue (red mud) in view of iron and selective rare earths recovery, *J. Sustain. Metall*. 2 (2016) 28–37. https://doi.org/10.1007/s40831-015-0026-4.
14. Frank Bullerjahn, Gerd Bolte, Composition of the reactivity of engineered slags from bauxite residue and steel slag smelting and use as SCM for Portland cement, *Constr. Build. Mater*. 321 (2022) 126331. https://doi.org/10.1016/j.conbuildmat.2022.126331.
15. Michiel Giels et al., High performance mortars from vitrified bauxite residue; the quest for the optimal chemistry and processing conditions, *Cem. Concr. Res*. 155 (2022) 106739.
16. Christina Siakati et al., Unraveling the nano-structure of a glassy CaO-FeO-SiO2 slag by molecular dynamics simulations, *J. Non. Cryst. Solids*. 528 (2020) 119771. https://doi.org/10.1016/j.jnoncrysol.2019.119771.
17. Bjorn Mysen, Pascal Richet, *Silicate glasses and melts*, 2018. https://doi.org/10.1016/C2018-0-00864-6.
18. EN 196-6, *Methods of testing cement* - Part 6: Determination of fineness, 2010.
19. François Avet et al., Development of a new rapid, relevant and reliable (R3) test method to evaluate the pozzolanic reactivity of calcined kaolinitic clays, *Cem. Concr. Res*. 85 (2016) 1–11. https://doi.org/10.1016/j.cemconres.2016.02.015.
20. Xuerun Li et al., Reactivity tests for supplementary cementitious materials: RILEM TC 267-TRM phase 1, *Mater. Struct. Constr*. 51 (2018). https://doi.org/10.1617/s11527-018-1269-x.

21. ASTMC1897-20, *Standard Test Methods for Measuring the Reactivity of Supplementary Cementitious Materials by Isothermal Calorimetry and Bound Water Measurements*, 2020. https://doi.org/10.1520/C1897-20.2.
22. EN 196-1, *Methods of testing cement* - Part 1: Determination of strength, 2016.
23. M. Gräfe, G. Power, C. Klauber, Bauxite residue issues: III. Alkalinity and associated chemistry, *Hydrometallurgy*. 108 (2011) 60–79. https://doi.org/10.1016/j.hydromet.2011.02.004.
24. C.W. Bale et al., FactSage thermochemical software and databases - recent developments, Calphad Comput. Coupling Phase Diagrams *Thermochem*. 33 (2009) 295–311. https://doi.org/10.1016/j.calphad.2008.09.009.
25. Karen Scrivener, Ruben Snellings, Barbara Lothenbach, *A Practical Guide to Microstructural Analysis of Cementitious Materials*, 2016.
26. Fabien Georget et al., Stability of hemicarbonate under cement paste-like conditions, *Cem. Concr. Res*. 153 (2022) 106692. https://doi.org/10.1016/j.cemconres.2021.106692.
27. Vincent Hallet et al., Hydration of blended cement with high volume iron-rich slag from non-ferrous metallurgy, *Cem. Concr. Res*. 151 (2022) 106624. https://doi.org/10.1016/j.cemconres.2021.106624.
28. T. Matschei, B. Lothenbach, F.P. Glasser, The role of calcium carbonate in cement hydration, *Cem. Concr. Res*. 37 (2007) 551–558. https://doi.org/10.1016/j.cemconres.2006.10.013.
29. M. Antoni et al., Cement substitution by a combination of metakaolin and limestone, *Cem. Concr. Res*. 42 (2012) 1579–1589. https://doi.org/10.1016/j.cemconres.2012.09.006.